THERMOELECTRIC PROPERTIES OF Sr DOPED $Ca_3Co_4O_9$ CERAMIC METERIAL

A Thesis

Submitted in partial fulfilment for the award of degree of

INTEGRATED MASTERS OF SCIENCE IN PHYSICS

Submitted by

GUGLOTH NAVEEN

(Reg. No.: I190413)

Under the guidance of

Dr. K. MOHANRAJ

(Associate Professor)

DEPARTMENT OF PHYSICS

SCHOOL OF BASIC AND APPLIED SCIENCES

CENTRAL UNIVERSITY OF TAMIL NADU

THIRUVARUR

MAY 2024

DECLARATION

This is to certify that this project thesis entitled " **THERMOELECTRIC PROPERTIES OF Sr DOPED $Ca_3Co_4O_9$ CERAMIC METERIAL** " which is submitted by me in partial fulfilment of the requirements for the award of the degree **INTEGRATED MASTERS OF SCIENCE IN PHYSICS** to the Central University of Tamil Nadu, comprises only my original work and due acknowledgement has been made in the text to all other materials used.

Date: **Signature of the candidate**

Place: Thiruvarur **(Gugloth Naveen)**

तमिलनाडु केन्द्रीय विश्वविद्यालय

(संसद द्वारा पारित अधिनियम 2009 के अंतर्गत स्थापित)

CENTRAL UNIVERSITY OF TAMIL NADU

(Established by an Act of Parliament, 2009)

CERTIFICATE

This is to certify that this project entitled "" **THERMOELECTRIC PROPERTIES OF Sr DOPED $Ca_{3-x}Co_xO_9$ CERAMIC METERIAL** " submitted in partial fulfilment of the degree of **INTEGRATED MASTERS OF SCIENCE IN PHYSICS** to the Central University of Tamil Nadu, done by **GUGLOTH NAVEEN**, Register No.: **I190413**, is an authentic work carried out by her at Department of Physics, Central University of Tamil Nadu under my guidance. To the best of my knowledge and belief, the content presented in this project has not been previously submitted for the attainment of any degree.

Date:
Place: Thiruvarur

Dr. K. Mohanraj
Project Supervisor

Head of the Department

Dr. K. C. Chandra shekar
Project Co-Ordinator

ACKNOWLEGMENTS

I wish to extend my heartfelt gratitude and special recognition to my Project Supervisor **Dr . K. Mohanraj**, Department of Physics, Central University of Tamil Nadu for providing me this opportunity. I would also like to express my sincere gratitude for his patience, mentorship, motivation and encouragement throughout my project period. I am very grateful to have worked in his project group. I would like to thank him for providing me a good environment to nurture my ideas.

My sincere thanks to Dr. P. Ravindran, Head of the department central university of Tamil Nadu For his talented Advice and providing necessary facility for my work

I want to thank **Mr. Charan** and **Mr. Akash** for helping me from the beginning. And I will also like to acknowledge that they never get tired of helping me whenever the needs arise.

I would also like to thank the Research Scholars, **Mr. Mangalapuri govardhan**, for his help and guidance. I am also thankful to my colleagues **Mr. R.S prakathes mara**n and **Mr. vigneshvaran** for their support and help in this project.

I extend my gratefulness to **Mr. Sultan Ibrahim**, Lab Technical assistance, **Mr. Dhanraj** and **Mr. Prabhu** lab assistance, Department of physics for timely issues of lab equipment and chemicals whenever there was needed.

I would also like to show my gratefulness to my other **friends** for making my stay in this university a pleasant experience, I also extend my thanks to other classmates for their help and encouragement during the tenure of this project

ABSTRACT

In this project, we prepared $Ca_{3-x}Co_xO_9$ Ceramic sample were prepared through solid state reaction method. The structural and thermoelectric property of polycrystalline samples of Sr doped $Ca_{3-x}Co_xO_9$ will be analysed using X-Ray diffraction. Electrical conductivity and Seebeck coefficient studies. the peaks were corresponding to monoclinic structure of CCO with space group C1M1 (JCPDS No:062-0692) Power factor value will be evaluated from electrical conductivity and Seebeck coefficient. Electrical conductivity value found to be increased with Sr substitution given to observed around 700 ^{0}C for $Ca_{2.75}Sr_{0.25}$ Co_4O_9 Seebeck coefficient of found to be increasing with Sr Substitution give to its directly depends on carrier concentration. The maximum value of Power factor of $1.4mW^{-1}k^{-2}$.its is for x is 0.75 measuring at 700 ^{O}C.

CONTENTS

CHAPTER 3: RESULTS AND DISCUSSION

CHAPTER 4: CONCLUSION

CHAPTER 1

INTRODUCTION

Recent years have seen the completion of massive research programmes aimed at supplying the energy needed for our continued existence. Non-renewable energy resources belong to one of the two categories: renewable and non-renewable, such as fossil fuels, are used more frequently in the former category. When fossil fuels are used for extended periods of time, the climate is negatively impacted, resources are depleted, and the environment suffers. Fossil fuels are created by the decomposition of plants and animals. These fuels, which originate from the Earth's crust, contain hydrogen and carbon, which when burned, produce energy. Among the fossil fuels are natural gas, coal, and oil, and natural gas.

The finite nature of renewable energy sources underscores the urgency to limit our consumption, as their depletion looms closer. Pollution, predominantly stemming from fossil fuels, poses a pressing concern. A major drawback of fossil fuels lies in their significant contribution to greenhouse gas emissions, with potential harm resulting from irresponsible usage.

A critical challenge we face today revolves around the scarcity of clean, renewable energy sources free from greenhouse gas emissions. Fossil fuels not only release harmful gases contributing to global warming but also generate pollution. Thermoelectric (TE) materials offer a promising solution by converting heat into electricity, enhancing fuel efficiency, and serving as a resilient alternative energy source across various applications. The utilization of thermoelectric modules in air conditioning stands out as an environmentally sound choice devoid of hazardous emissions. Notably, thermoelectric cooling systems boast several advantages over conventional counterparts, including enhanced reliability, elimination of working fluids, compact size, lightweight design, and the absence of mechanical moving parts.

1.1REVIEW OF THERMOELECTRIC METERIALS (TE)

The history of thermoelectric materials spans approximately two centuries, with extensive exploration dating back to the 19th century. Various materials, including Chalcogenide alloys, Half-Heusler alloys, Skutterudites, Clathrates, and Perovskites, have been subject to thorough investigation in this field. These materials have been categorized into three generations based on their figure of merit (ZT) and efficiency levels. Initially, the first generation exhibited a ZT of approximately 1 and efficiency ranging between 4% to 5%. With advancements introducing size effects, the second generation achieved a ZT of around 1.7 and an efficiency of approximately 11% to 15%, while the third generation pushed ZT to 1.8 with a power conversion efficiency of 15% to 20%. Notably, since the 1950s,$Bi_{2,}$ Ti_3PbTe and Bi-Te have been the most commonly utilized thermoelectric materials, notably deployed in radioisotope thermoelectric generators during the Apollo missions and later in the 1990s.

The advent of nanoscience has facilitated the downsizing of inorganic material dimensions, aiming to minimize heat conductivity and enhance thermoelectric power, Among various classes of thermoelectric materials, ceramics stand out for their unique combination of properties, including high-temperature stability, chemical inertness, and tunable electrical and thermal conductivity. The synthesis and identification of new ceramic compounds with improved thermoelectric characteristics represents one noteworthy advancement. A broad variety of ceramic compositions, including as oxides, sulphides, selenides, and tellurides, have been investigated by researchers in an effort to find materials with high thermoelectric figure of merit (ZT) values.

The ability to manipulate grain size, grain boundary scattering, and phonon scattering mechanisms in ceramic thermoelectric materials has been made possible by developments in nanostructuring techniques. Chemical vapour deposition, ball milling, and spark plasma sintering are examples of nanostructuring techniques that have been used to create nanostructured ceramics with enhanced thermoelectric qualities. In comparison to their bulk counterparts, these nanostructured ceramics have higher ZT values due to their decreased thermal conductivity, increased electrical conductivity, and increased Seebeck coefficient.

1.2 THERMOELECTRIC

Thermoelectric materials play a crucial role in converting heat into electricity, offering opportunities for primary power generation and energy conversion. These materials exploit three main thermoelectric effects: the Seebeck effect, the Peltier effect, and the Thomson effect. Notably, a significant portion of energy, approximately 60%, is lost as heat. The primary goal is to harness this wasted heat through technologies like thermoelectric generators (TEGs), extensively utilized in spacecraft, automobiles (such as GM and BMW), industrial processes, maritime vessels, and remote sensing applications in sectors like oil, gas, and nuclear industries.

A typical thermoelectric generator comprises alternating n-type and p-type semiconductor legs connected in series to an applied electric field and in parallel to the heat gradient. It operates based on fundamental thermoelectric principles. Semiconductor materials are favored for thermoelectric applications due to their superior properties compared to metals.

The popularity of thermoelectric devices surged with the discovery of suitable semiconductor materials, highlighting the critical role of semiconductors in advancing thermoelectric technologies.

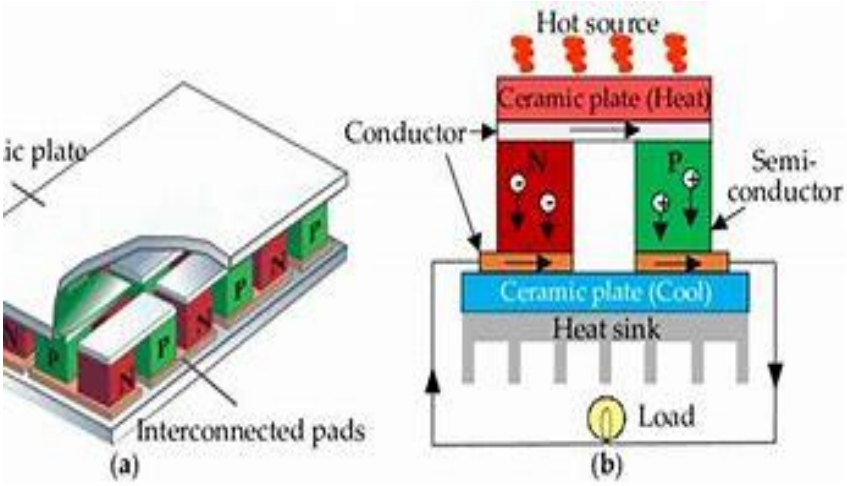

FIG:1 Schematic diagram of thermoelectric generator (TEG)

Metals were previously used as thermoelectric materials, but their efficiency was limited because metals' band structures were not conductive to charge (electron) transport because Fermi energy is found in the conduction band, where charge density is higher, and thus resistivity rises as temperature rises. Semiconductors, on the other hand, have a favorable band structure for charge carrier (electron and hole) transport and a negative temperature coefficient of resistivity, indicating that as temperature rises, their conductivity rises as well. Metals have a relatively low Seebeck coefficient in comparison to semiconductors. All of this indicates that actual thermoelectric materials are semiconductor materials.

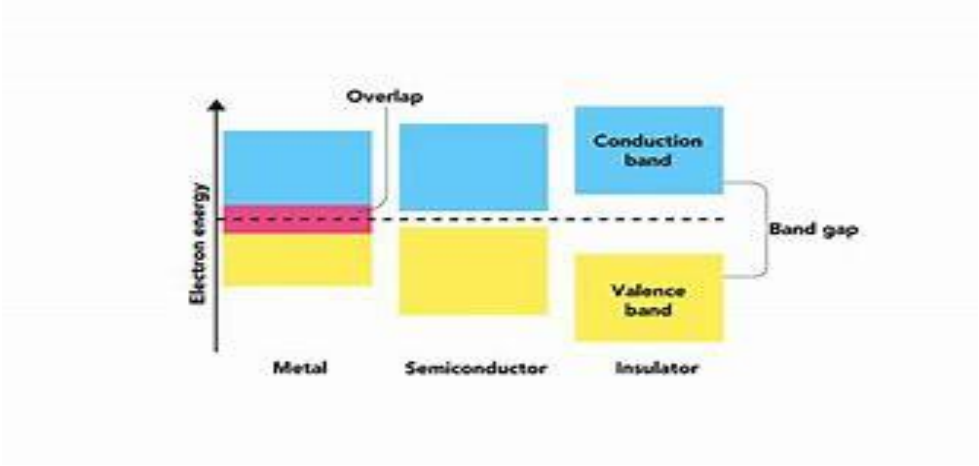

Fig:2. Band structure of metal, semiconductor, insulator

Thermoelectric devices are gaining popularity due to their environmentally benign energy conversion technique, high dependability and feasibility over a wide temperature range, and the lack of moving elements such as compressors or pumps, which makes them ideal for remote applications.

1.3 THERMOELECTRIC EFFECTS

Seebeck Effect:

In 1821, the German physicist Thomas Seebeck made a groundbreaking discovery: when two junctions composed of different metals or semiconductors are maintained at varying temperatures, a voltage is produced. This voltage, known as thermoelectric voltage, is a result of the Seebeck effect. The Seebeck Coefficient (S), also referred to as Thermopower, quantifies the magnitude of the voltage generated in the circuit. which is determined by the materials employed and the temperature differential produced ΔT.

Seebeck coefficient is given by

$$S = \frac{\nabla V}{\nabla T} \tag{1}$$

S=Seebeck's coefficient, ΔV =Electrostatic potential, ΔT = Temperature difference

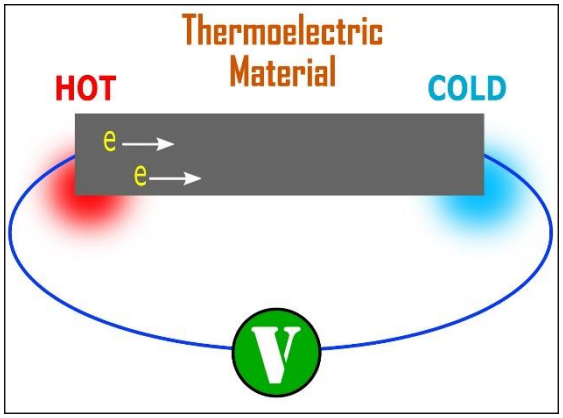

Fig:3 seebeck's experiment

Thomson Effect:

The Thomson effect, named after Scottish physicist William Thomson (also known as Lord Kelvin), is a thermoelectric phenomena that happens when an electric current travels through a conductor while a temperature gradient exists along its length. The Thomson effect differs from the Seebeck effect in that it requires a temperature gradient parallel to the direction of current flow rather than a temperature gradient perpendicular to it.

When an electric current passes through a conductor with a temperature gradient, heat is either absorbed or released at the points where the current enters or exits the conductor, depending on the direction of the temperature gradient. This heat exchange is a result of the interaction between the flow of charge carriers (electrons or holes) and the temperature gradient.

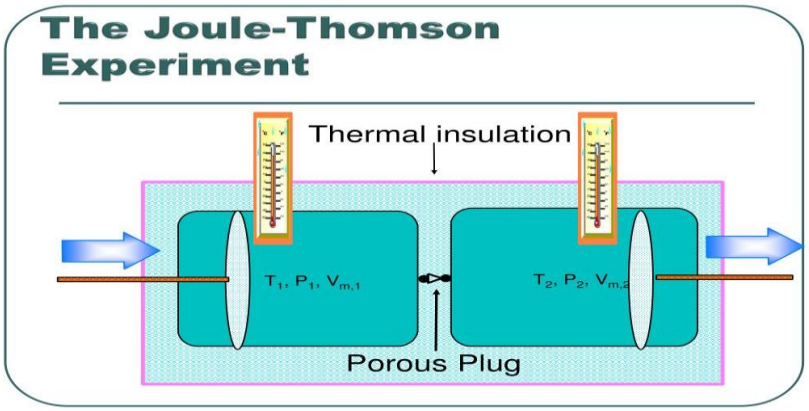

Fig :4: Joule-Thomson experiment

Peltier Effect:

The pelter effect is a thermoelectric phenomenon discovered in 1834 by french physicist jean Charles Athanase peltier.
When an electric current flow across a circuit made by two dissimilar metals, heat is absorbed or released at the junction, according to Jean Peltier, a French watchmaker. Seebeck's inverse effect is the Peltier effect. The Peltier effect is used to operate thermoelectric cooling devices (refrigerators).

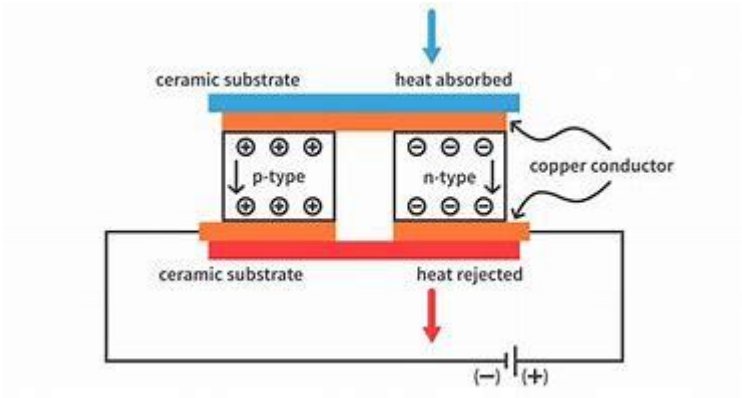

Fig :5 Peltier Effect

1.3.1 Efficiency of Thermoelectric materials and its Interdependency.

The Efficiency of the thermoelectric materials is characterized by a dimensionless quantity known as figure of merit (ZT). It is given by the following equation

$$ZT = \frac{s^2 \sigma T}{k} \quad (2)$$

In the above equation,

- S denote Seebeck coefficient
- σ indicate Electrical conductivity (Sm^{-1}) which is the measure of a material's ability to allow the transport of an electric charge.
- Power factor PF= $S^2\sigma$ on the numerator in equation (2) characterizes the electron energy conversion capability.
- Thermal conductivity, denoted by the symbol κ(W/k), characterizes the efficiency of heat transfer via conduction across a material's unit cross-sectional area when there's a perpendicular temperature gradient. This property encompasses both electronic and lattice contributions to heat conduction. $K=K_e + K_L$ (3)

Where K_e is the electronic thermal conductivity and K_L is the lattice Thermal Conductivity . Weidemann-Franz relationship relates the Ke and σ as

$$K_e = \frac{\pi^2 K^2 B}{3e2} \sigma T = \mathbf{L}\, \sigma T \quad (4)$$

Where Lorentz number(L), electrical conductivity(σ) and Temperature(T). It characterizes heat leakage. According to General Ohm's law electrical conductivity can be expressed as

$$\sigma = \frac{1}{R} = \eta e \mu \quad (5)$$

This proves that the electronic contribution of thermal conductivity is depends on the thermal carrier concentrations. However the lattice contribution of thermal conductivity does not depends on the carrier concentration which can be expressed as

$$K_L = \frac{1}{3} C_\upsilon \nu \iota \quad (6)$$

Where heat capacity per unit volume(C_υ) , the average phonon velocity(ν) and is ι the phonon mean free path. It shows that for a good thermoelectric materials, thermal conductivity by phonon contribution should be preferred as it does not involves the carrier concentration thereby it will not affect the electrical conductivity. Figure 6 represents semiconductors are the

true thermoelectric materials whereas a metal has thermal conductivity dominated by electronic contribution which directly causes ZT and an insulator has no remarkable electrical conductivity.

Pisarenko relationship relates S and n as below

$$S = \frac{8\Pi^2\kappa^2 B}{3eh^2}\ m\ *\ T\left(\frac{\pi}{3\eta}\right)\frac{2}{3} \tag{7}$$

Where K_B is Boltzmann constant and charge(e), h is planks constant, m* is effective mass and n is Carrier concentration. From the above equation we can say that S is inversely dependent on the carrier concentration n at constant temperature.

From the above equation we can conclude that the S and σ are inter related with the carrer concentration (n). σ Shows direct dependence on n whereas S shows indirect dependence. We can Understand that simultaneous increment of S and is not possible. σ This contradiction leads to poor power Factor. In addition to the contradiction, from the Weidemann-Franz relationship we can understand that the electronic contribution of thermal conductivity directly dependent on electrical conductivity which results into the simultaneous increment of K and σ, this is again questions the improvrmrnt of thermoelectric figure of merit (ZT).

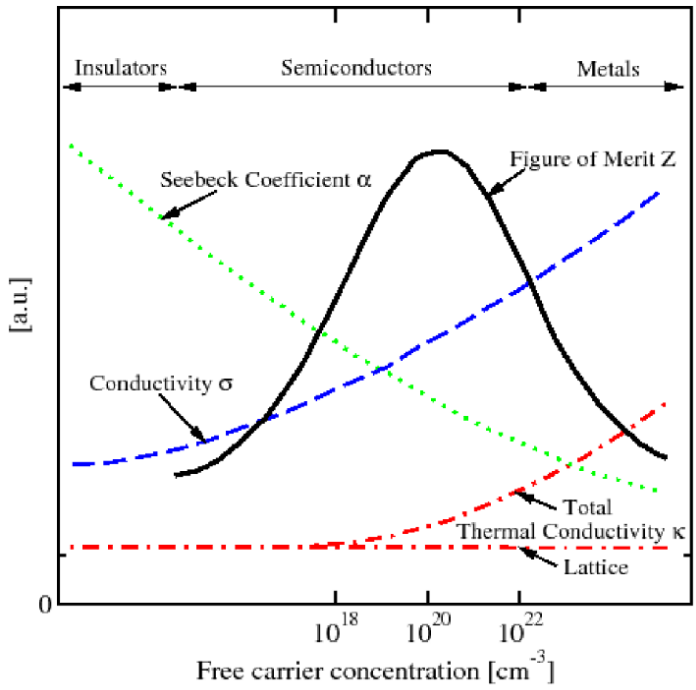

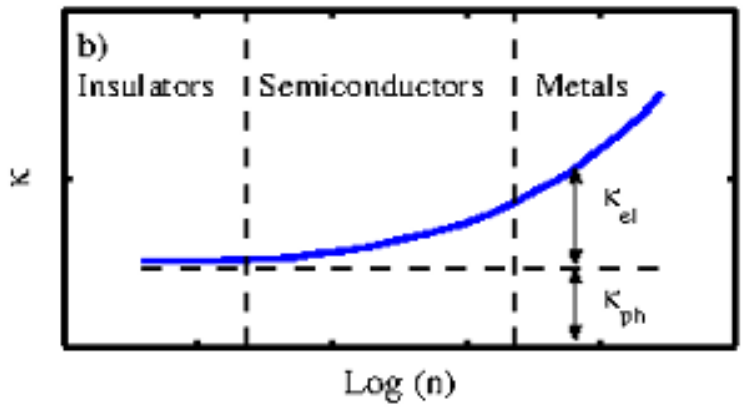

Figure :6 Relationship between carrier concentrations with all other thermoelectric parameter

The above figure which describes the relation between carrier concentration (n) with an essential thermoelectric parameters such as Seebeck Coefficient (S), Power factor ($S2\sigma$) , Electrical conductivity (σ) and thermal conductivity(k) and also it described the above arguments .

Achieving an optimal thermoelectric material poses a significant challenge, as it necessitates maximizing the power factor while minimizing thermal conductivity. However, these objectives often conflict with each other due to their inherently contradictory nature. This dilemma directly impacts the figure of merit (ZT), which quantifies the overall efficiency of a thermoelectric material. Balancing these opposing factors to enhance the ZT value presents a formidable challenge in thermoelectric research and development.

1.3.2 Calcium Cobalt oxide($Ca_3Co_4O_9$)

$Ca_3Co_4O_9$ offers notable benefits such as strong resistance to oxidation and excellent stability at high temperatures. However, its limited electrical conductivity results in inadequate thermoelectric performance. Hence, the figure of merit (ZT) of $Ca_3Co_4O_9$ materials falls short of meeting practical production requirements, necessitating modifications to enhance its thermoelectric properties. One effective approach involves doping the $Ca_3Co_4O_9$ material with additional elements. such as substitution at the Ca site, Co site, and combined doping at both sites. These approaches involve incorporating a diverse range of elements, spanning alkali (earth) metals, transition metals and rare earth metals, as well as main group metals and non-metals.

The Seebeck effect, recognized as the primary thermoelectric phenomenon, describes the generation of a voltage differential due to variations in temperature between distinct conductive or semiconductive materials. The Energy filtering effect serves to enhance the Seebeck coefficient by hindering low-energy carriers, while band engineering is commonly employed to optimize this coefficient through modifications in band structures, including resonant band levels and band convergence. Through strategic adjustments in doping elements and doping levels, resonant levels can be attained, consequently increasing the density of states and augmenting the Seebeck coefficient. Band convergence occurs when multiple bands exhibit

comparable energy levels, further contributing to the enhancement of thermoelectric performance.

Considering the definition of the figure of merit (ZT), achieving a high ZT value at a specific temperature necessitates either a high Seebeck coefficient (S), high electrical conductivity (σ), large power factor (PF), and/or low thermal conductivity (κ). Enhancing electrical conductivity (σ) is often achieved through doping with p-type or n-type impurities. Nonetheless, this may lead to reduced carrier mobility due to impurity scattering effects. To overcome this limitation, modulation doping can be employed to spatially separate the carriers from their matrix materials, thereby promoting high carrier mobility.

The preparation of $Ca_3Co_4O_9$ materials is adopted solid state synthesis method , sol-gel method, and so on. The solid-state reaction involves mixing metal oxides or inorganic salts (e.g., nitrates, carbonates) in a stoichiometric ratio and calcining them at high temperatures to produce a specific component material. Sintering is the crucial part. Multiple high-temperature sintering procedures are typically necessary due to the high energy required for nucleation and diffusion.

1.3.3 Application of Thermoelectric materials

1. Refrigerators made from thermoelectric materials are known as "thermoelectric coolers" or "Peltier coolers" due to the Peltier effect that controls their operation. Peltier cooling is not as widely used as vapor-compression refrigeration. Peltier coolers have several advantages over vapor-compression refrigerators, including no moving parts or refrigerant, minimal size, and flexible shape.

2. Thermoelectric devices requiring minimal thermal energy, such as those integrated into wearable and medical devices for human use, can benefit from its supply.

3. Wireless sensor networks (WSNs) manage wireless communication within sophisticated sensor networks. Presently, these systems rely on disposable batteries, which emit harmful chemicals upon disposal (such as Pb, Cr, Cd, etc.). The development of battery-free WSNs holds significance for the integration of eco-friendly technologies into future industries.

4. The automotive industry faces challenges from expensive fuel and high carbon dioxide (CO2) emissions, prompting exploration of novel solutions to enhance engine performance. Presently, numerous companies (e.g., BMW, Honda, etc.) are actively exploring thermoelectric generators (TEGs) as a potential remedy [9, 21, 64]. Contemporary research endeavors focus on the development of TEGs capable of converting waste heat from internal combustion, typically expelled through engine exhaust, into usable electrical energy for commercial vehicles.

5. Thermoelectric generators (TEGs) designed for aerospace applications, particularly radioisotope thermoelectric generators (RTGs), are commonly deployed in spacecraft, satellites, and space probes. These devices harness the heat produced by the natural decay of radioactive materials to generate electricity. Various isotopes, including Cerium-144 and Polonium-210, have been utilized over time, but Plutonium-238 remains the preferred choice due to its advantageous properties: a high melting point, minimal gamma radiation emission, and an extended half-life of nearly 90 years, rendering it ideal for sustained operation in such environments.

Power generation and thermoelectric generator

1. The figure of merit, or ZT, influences thermoelectric efficiency. ZT has no theoretical upper limit, and its thermoelectric efficiency approaches the Carnot limit as it approaches infinity. Until recently, there was no known thermoelectric with a ZT > 3. In 2019, researchers announced with a ZT of approximately 5 to 6.

2. As of 2010, thermoelectric generators are used in applications where dependability, light weight, and tiny size are more critical than efficiency and cost.

3. Cogeneration power plants repurpose the heat generated during electricity generation, making them more profitable in industries that generate a lot of waste energy.

4. Internal combustion engines currently capture only 20-25 percent of the energy generated during fuel combustion. Enhancing this conversion rate holds the potential to enhance fuel efficiency and additionally supply surplus electricity for on-board functionalities and amenities, including stability controls, telematics, navigation systems, and electronic braking systems. Such improvements could potentially redirect the engine's energy usage, in specific scenarios, towards powering the car's electrical components, such as electric power steering or coolant pump operation.

5. Thermoelectric technology could be used in such systems or to generate solar thermal energy

6. Among the various static energy conversion methods explored for radioisotope power systems in space applications, thermoelectric (TE) energy conversion has garnered significant attention. Radioisotope thermoelectric generators (RTGs) operate by harnessing the heat emitted from the nuclear decay of radioactive isotopes, typically plutonium-238, and converting it into electricity. RTGs have effectively powered numerous space missions, including the Apollo lunar missions, Viking Mars landers, and the International Space Station, as well as outer-planet spacecraft such as Voyager, Ulysses, Galileo, and Cassini, along with Pioneer 10 and 11. These generators are characterized by their compactness, durability, radiation resistance, scalability, and demonstrated reliability over extended periods, spanning decades. They operate silently, without vibration or torque, making them well-suited for autonomous missions in space and on planetary surfaces. Utilizing temperature gradients, TE materials generate a voltage known as the Seebeck voltage within converter units. The current state-of-the-art RTGs achieve a system conversion efficiency of approximately 6%. Notable TE materials for these applications include bismuth telluride (Bi2Te3) and lead telluride (PbTe). Despite advancements in vehicle emission control and fuel efficiency, the proliferation of motor vehicles on U.S. roads and the cumulative mileage driven by these vehicles persistently escalate, leading to heightened air pollution, greater petroleum consumption, and increased dependence on foreign petroleum sources. To mitigate these trends, it is imperative to implement new automotive technologies aimed at enhancing fuel economy without exacerbating harmful emissions

1.3.4. Solid state reaction

The synthesis of polycrystalline bulk ceramics involves a solid-state process, necessitating a diverse range of starting materials such as carbonates and oxides. Since these solids remain inert at ambient temperatures, they must be subjected to elevated temperatures to initiate the

reaction. This method holds significance from both kinetic and thermodynamic perspectives. At elevated temperatures, the solid precursors chemically react without the need for a solvent, yielding a stable end product. A notable advantage of this approach is the structural purity and requisite qualities inherent in the resulting solid component. The solid-state synthesis reaction is delineated into distinct steps, each characterized by its own set of considerations and intricacies.

At high temperature the solid precursors undergo chemical transformation without the presents of any solvent, This leads to the creation of a stable and structurally pristine final product. The omission of solvents alleviates worries regarding impurities and the need for solvent extraction, simplifying the synthesis method.

The advantages that offers a solid state synthesis are scalability, reproducibility, by adjusting the process parameters such as temperature, duration, and precursor composition we can tailor the property of the materials. Moreover, it provides the opportunity to introduce dopants or additives for adjusting the properties of the ceramic, thereby enhancing the flexibility in material design.

The solid state synthesis involves several steps such as, choosing precursor, heating, intermediate phase formation, and final ceramic consolidation, for each step require careful observation of factors such as homoginity of mixture, particle size distribution, reaction kenetics, and thermodynamic stability to ensure the final product is formed or not.

1.3.5 Choosing Of Precursors

Precursors are the starting raw material also called as regents. The nature of the raw materials has a major effect on the properties of the finals ceramic material. The starting reagents have to dry before weighting in order to remove the moisture and are to be selected on the basic of reaction conditions. They have to be taken in appropriate stoichiometric ratio for the formation of desired product. selecting precursors Is the more complicated thing the selected materials should satisfy the property that we need.

1.3.6. Ball milling

Mechanical milling employs mechanical force, typically compressive, to effectively reduce the particle size of bulk materials. This process, also known as mechanical alloying or ball milling, is commonly utilized to reduce grain sizes to the nano regime. Nanostructures are achieved through repetitive mechanical deformation and alloying as the material is vigorously agitated in a container containing milling balls. Energy transfer to the powder occurs through shearing action or the impact of high-velocity balls with the powder. Various factors, such as milling speed, equipment type, ball size, and ball-to-powder weight ratio, influence the particle size of the powder. A key aspect of mechanical milling is the collision between the balls and powder particles, leading to deformation and fracture, ultimately defining the resulting powder structure. The ratio of powder to balls typically ranges from 1:5 to 1:10, depending on the desired particle size.

1.3.7 Calcination

Following the milling process, the precursor mixture requires calcination to determine the appropriate temperature. This temperature can be estimated through thermal analysis techniques such as DSC/TGA, applied to the dried precursor mixture. Throughout calcination, compound phase formation occurs via solid-phase reactions, involving chemical reactions facilitated by atomic diffusion at temperatures below the precursors' melting points.

1.3.8 pelleting

The principle behind pelleting processes is the opposite of grinding technology. It involves compaction of fine solid. For the application of thermodynamic there will be different type diameters(mm),There are two main pelletizing methods;

- **Wet agglomeration:** In wet agglomeration, particle cohesion is achieved by introducing a binding liquid (typically water, although organic or chemical agents like Poly Vinyl Alcohol can also be utilized) and employing mechanical forces from a suitable apparatus (such as pelleting discs, rectangular or granular mixers). Compression is deliberately avoided to maintain pellet stability.
- **Dry agglomeration:** Dry agglomeration, on the other hand, involves forming pellets through compression, where cohesion is achieved by reducing particle spacing and enhancing their contact surface. No binders are used in this process.

The efficiency of the operation often depends on the mechanical stability of formed pellets

1.3.9 Sintering

Sintering involves heating of the powder compact at a temperature less than the melting point of the material for acquiring appreciable density. The mechanism involved in the enhancement of density is diffusional mass transport. The various mechanisms of sintering of polycrystalline material take place through bonding growth of necks between the particles; various sintering mechanisms are lattice diffusion from the surface, diffusion vapor transport, lattice diffusion from the grain boundary diffusion, and plastic flow. Grain boundary diffusion and lattice are the most important densification mechanisms in the polycrystalline ceramics. The diffusion from grain boundary to the the pore permits neck growth as well as the densification process. Besides these mechanisms, different ionic species forming the compound are heated to a temperature, which is approximately ~50 − 80% of the melting temperature, as a results pellet does not melt and the particle size in to reduce the porously of the compact by ionic diffusion

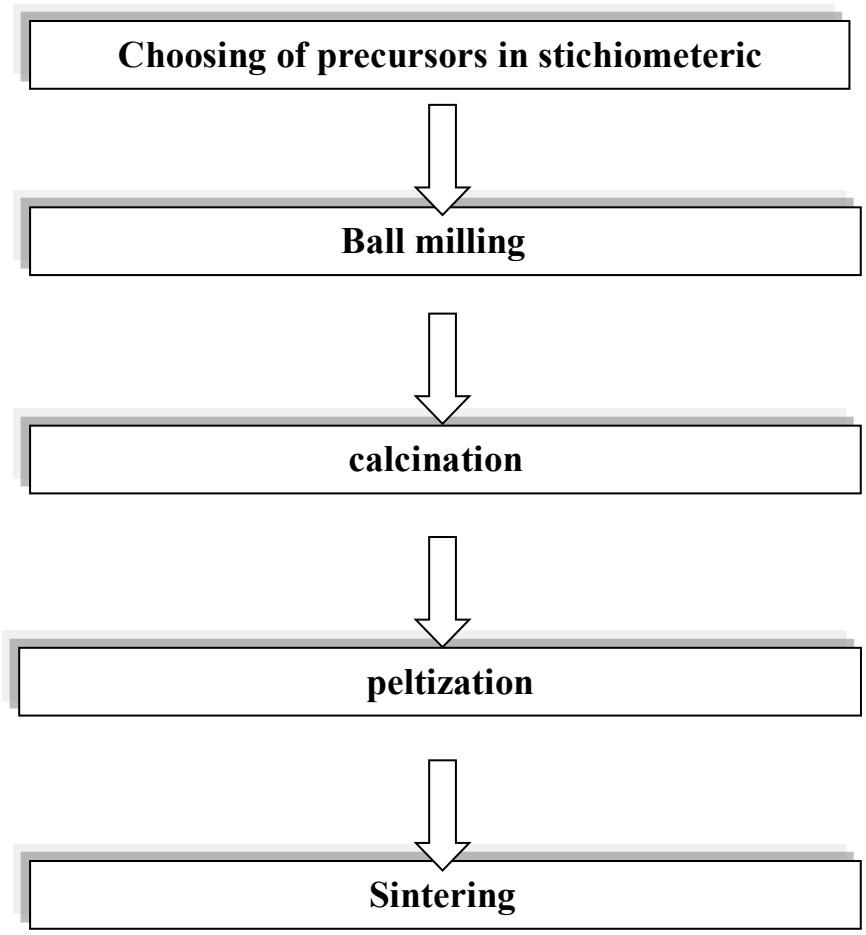

Fig 7: Schimatic diagram of Solid sate synthesis

CHAPTER 2

2. SYNTHESIS AND CHARACTERIZING TECHNIQUES

2.1 SYNTHESIS OF DESIRED MATERIAL

In order to get the desired result, we used a solid-state reaction method. Product. It entails a number of steps, which are outlined below.

1.Weigh the initial raw materials in the correct stoichiometric ratio, which is critical during the reaction. We used as a starting point material.

Concentration(x)	CaCo3	Co2O3	SrCo3
0	1.80171	1.80192	0
0.25	1.4334	5.3627	0.4227
0.5	1.2612	5.3949	0.6701
0.75	1.0968	5.2767	0.807

Table 1: This table shows the different type of concentration of the composition

2. Another crucial condition for this sort of reaction is the container, or crucible, to exclude undesired impurities. We employed a Zirconium jar, Zirconium balls, and an Agate motor for grinding and mixing, and Alumina crucibles for calcination and sintering since they are stable at high temperatures.

3. Throughout the mixing process, grind the beginning materials in a planetary ball-mill with the addition of ethanol and acetone in an appropriate ratio and a standard ball powder ratio (B:P) of 10:1 at a speed of 300 rpm for 40 minutes with a stop of 10 minutes. Wet grinding is preferred over dry grinding because it is easier to achieve a homogenous mixture and minimize particle size. After the grinding is completed, the wet mixture is placed in a hot-air oven to evaporate the ethanol, at the temperature 120 c for overnight.

4. To obtain the desired result, the obtained powder must be calcined after drying. Calcination is the heat treatment of the reactants to remove volatile compounds, either in an inert atmosphere at 700°C for 7hr hours

5. The re-milled materials were then dried again, as detailed above, to evaporate the ethanol. The result was then transformed into pellets of various sizes using an agate mortar for manual intermediate grindings for characterization tests. With the use of a uniaxial press, pellets of 15mm, were created. For 8 minutes, a pressure of 8Mbar was applied.

6. After that, the pellets were sintered at 800°C for 7 hours at a rate of 5°C/min in O2 atmosphere. Sintering is also a heating process that takes place at a specific temperature, for a specific amount of time, and in a specific environment. When the powder compacts, this

process happens; the temperature utilized in this process should be below the melting point of the material, this temperature is used to nucleation in the pellet.

7. The obtained pellets are next inspected for quality, such as smoothness, lack of cracks, and good density, before being used for characterization such as Archimedes XRD, and thermoelectric characteristics

2.2 CHARACTERIZATION TECHNIQUES USED

2.2.1 X-Ray Diffraction (XRD)

X-rays are essentially electromagnetic waves falling within the wavelength range of 10^-5 to 100, which aligns with the spacing between lattice planes within a crystal. These wavelengths are produced when electrons undergo inelastic scattering, losing energy in the process. The scattered waves can either align in phase, leading to constructive interference, or out of phase, resulting in destructive interference. X-ray diffraction relies on the constructive interference of monochromatic X-rays with a crystalline sample, with Bragg's law dictating the conditions for this constructive interference.

$$\eta\lambda = 2d\sin\theta \tag{8}$$

Where n is the integer can be defined as an order of wavelength, is wavelength, d is spacing between the crystal planes and is the angle of diffraction. Fig (8) explain Bragg's law θ further as below.

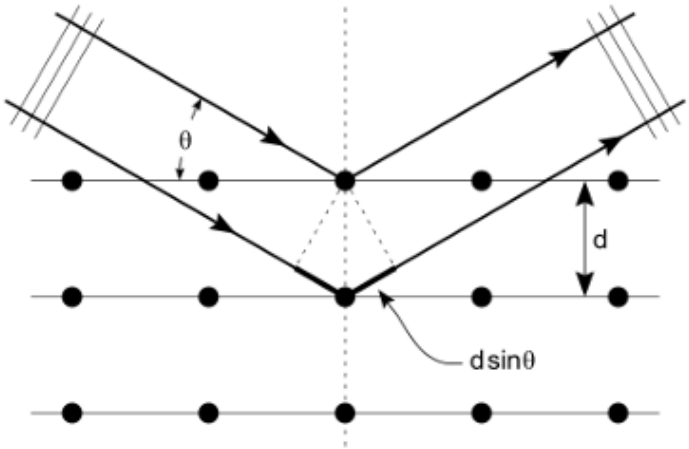

Fig 7. Bragg's law

X-ray powder diffraction differs from single crystal diffraction in that single crystals produce only one set of peaks in the diffraction pattern, whereas powder diffraction is conducted on polycrystalline samples, resulting in all possible diffraction patterns. These obtained patterns serve as unique fingerprints for each material, enabling comparison with standard powder diffraction files (PDFs) or databases for identification purposes. Peaks in the identified pattern provide valuable information such as the spacing between crystal planes ($d_{\_hkl}$) and intensities corresponding to different diffraction angles (2θ). This data allows for the identification of material phases and determination of unit cell dimensions.

The lattice spacing and parameters can be obtained from the relation

For a cubic system a=b=c

$$\frac{1}{d^2} = \frac{h^2+k^2+l^2}{a^2} \tag{9}$$

For an orthorhombic system a ≠ b ≠ c

$$\frac{h}{d^2} = \frac{h^2}{a^2} + \frac{k^2}{b^2} + \frac{l^2}{c^2} \tag{10}$$

Where a, b, c are the lattice parameters and h, k, l area the miller indices.

We studied our power sample with the help of PANalytical X-ray diffractometer with Cu Kα radiation of λ = 1.5418 A. with the scanning range of 5° to 90° .

2.2.2 Density Measurement

The Archimedes principle serves as the basis for calculating density using a digital weighing scale. This principle asserts that density, a physical property, is influenced by temperature and pressure. It provides insights into the weight of a substance, with heavier substances typically having higher densities when compared to identical ones.

Density determination often employs the buoyancy principle and buoyancy weighing. This involves submerging a sinking body in the liquid under examination and then calculating its buoyancy using a balance. By dividing the buoyancy by the volume of the sinking body, the density of the liquid can be estimated accurately. These principles find widespread application in determining the density of various unknown materials.

In our research, we employed an apparent weight loss technique. Apparent weight refers to the weight of an object measured when it is submerged in air. Utilizing the principle, we can infer that the apparent weight decreases when an object is immersed in a liquid, owing to buoyant force acting on it. This technique provides a practical means of estimating density in experimental settings (W_l) equals the weight of the fluid displaced (W_{fd})**.**

$$W_1 = W_{fd} \quad (11)$$

As we knpwn the density can be expressed as

$$\mathbf{P} = \frac{\boldsymbol{m}}{\boldsymbol{v}} \quad (12)$$

Where P is the density, m is the mass and v is volume.

Using the above two relation the density of unknown materials is found from the expression as follows

$$\text{Density of Unknown} = \text{Density of fluid} * \left(\frac{Wair}{Wl} \right)$$

Where W_{air} is the item weight in the air and W_1 is the apparent weight loss (W_1 =weight in air -Weight in the fluid), and the fluid we used is water with a density of 1.00g/cm^3

2.2.3 Measurement of Seebeck Coefficient and Electrical Conductivity

The schematic layout of the SBA 458 arrangement is depicted in Figure 9, where the furnace encompasses the entire measurement setup. The sample, indicated in blue, is centrally positioned on a ceramic sample support made of Al2O3. This support features micro heaters on both sides and accommodates two thermocouples and two current pins at the sample's base for determining the Seebeck coefficient and electrical conductivity.

The thermocouples and current pins are securely embedded within the ceramic sample support, with contact ensured by springs located in the device's cold region. These components remain permanently affixed to the support, maintaining continuous contact with the sample through the springs. To ensure consistent contact forces, the sample is pressed against the support using a pressure disc and weight.

The measurement procedure is fully automated, initiated by heating the furnaces according to a pre-set temperature schedule. Electrical conductivity and the Seebeck coefficient are initially measured at isothermal sites. This process is repeated for each defined temperature step. Upon completion of the measurement program, as the furnace cools down, the sample can be safely withdrawn. This automated procedure streamlines the measurement process and ensures reliable data collection.

Fig 9: the NETZSCH SBA 458 setup

2.2.4 Measurement of the electrical conductivity

Electrical conductivity measurement is conducted using the 4-point measurement method, as depicted in the diagram above. The setup involves two thermocouples and two current pins in contact with the sample, which rests on the sample support. The thermocouples, represented by blue and green wires, are positioned centrally on the lower side of the sample, while the current pins, indicated in red, are located on the outer edges.

This configuration allows for the application of current in two directions (positive and negative) through the sample. In each direction, three different current values are supplied: one-third of the maximum current value (1/3 Imax), two-thirds of the maximum (2/3 Imax), and the maximum current value (Imax). The measurement software enables the user to select Imax, with the software subsequently determining and supplying each of the three current values five times in both positive and negative directions to the sample.

Maintaining consistency in current application is crucial to avoid inaccuracies caused by sample heating during the measurement of electrical conductivity. The selection of Imax should be based on considerations such as the geometry and material of the sample to ensure optimal measurement conditions.

2.2.5 Measurement of the Seebeck coefficient

The two micro heaters integrated into the ceramic sample support, positioned on the left and right sides, are essential for measuring the Seebeck coefficient. These heaters generate a temperature gradient observable in both directions across the sample. Initially, one side of the sample is heated, followed by cooling, and then the opposite side undergoes the same heating and cooling process. Throughout this procedure, voltages UA, UB, UT1, and UT2 are monitored.

UA and UB represent the voltages measured between the positive and negative wires of the thermocouples. These voltages are compared to the temperature difference (delta T, denoted as T) between the two sides of the sample. Over 100 measurement points are recorded during the entire cycle, including the heating and cooling phases of both sample sides, to accurately calculate delta T.

If there's any lack of contact between the sample and the thermocouple, or if the sample exhibits characteristics of inhomogeneity, deviations from linearity (such as hysteresis) may be observed in both measurement curves. In such cases, an assessment of the measurement's quality can be made.

Using the provided formula, the Seebeck coefficient can be computed utilizing the gradients (aA and aB) of the two curves in the diagram. SA and SB represent the Seebeck coefficients of the materials A and B, corresponding to the positive and negative wires of the thermocouples, respectively.

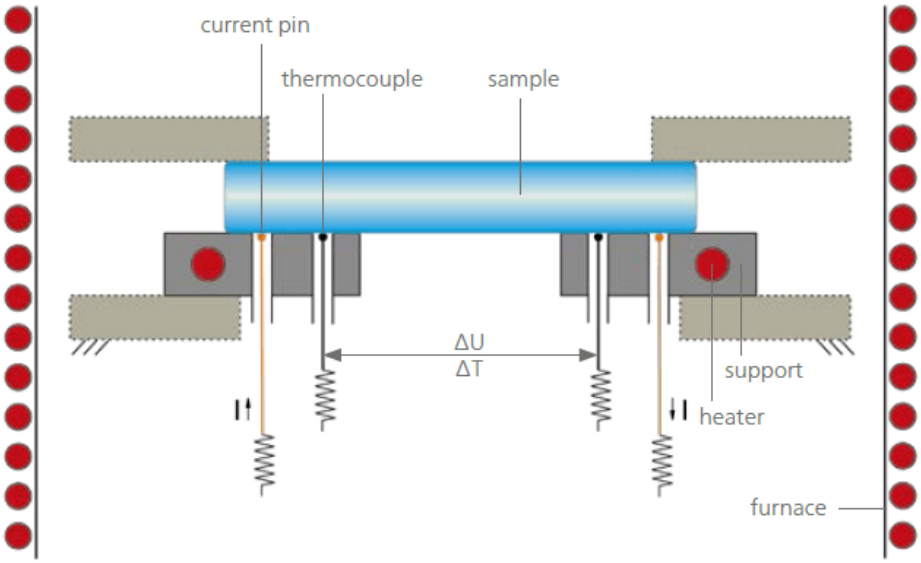

Fig 10: The schematic of the NETZSCH SBA 458 setup

CHAPTER 3

RESULTS AND DISCUSSION

Polycrystalline samples of Sr doped $Ca_3Co_4O_9$ samples were synthesized successfully using solid state reaction. We have performed X-Ray Diffraction studies and thermoelectric studies-simultaneous measurement of electrical conductivity and Seebeck coefficient in order to analyze its structural, transport and thermoelectric properties. Power factor values were evaluated from electrical conductivity and seebeck coefficient. The characterizations performed are discussed below.

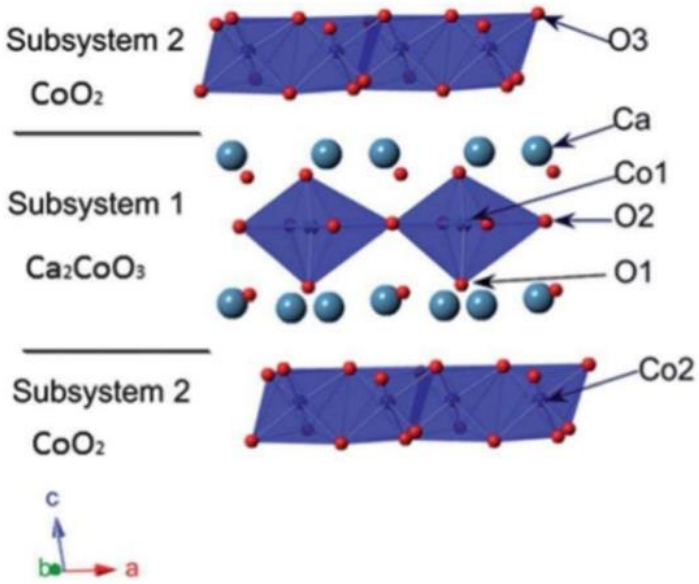

Fig 11: crystal structure of $Ca_3Co_4O_9$

3.1. X-RAY DIFFRACTION

The powder X-ray diffraction (XRD) pattern $Ca_{3-x}Sr_xCo_4O_9$ sample are displayed in fig:10. it is used to investigate the phase purity and establish phase relationships. data have been collected using 2θ scanning range from 10^0 to 60^0. In this graphs it is clear that all the samples have very similar diffraction pattern.in all the case major peaks are associated to the thermoelectric $Ca_3Co_4O_9$ (x= 0, 0.25, 0.5, 0.75) sample at room temperature, from the graph the structure of the compound is Monoclinic with the space group C1M1 (JCPDS: 062-0692). All the samples are shown single phase with no trace of impurity. There is a slight shift absorber in (002) peak which indicates that the Sr was successfully doped into $Ca_3Co_4O_9$ lattice.

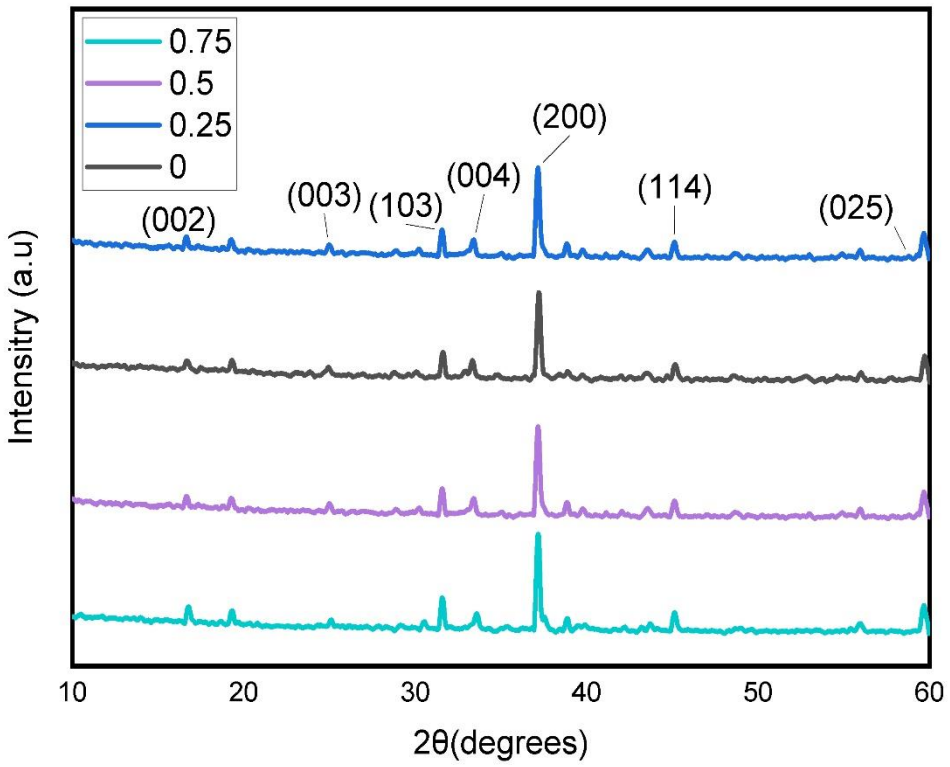

Fig 12. XRD pattern of $Ca_{3-x}Sr_xCo_4O_9$ (x=0, 0.25, 0.5, 0.75) at room temperature

3.2 ELECTRICAL CONDUCTIVITY

Electrical conductivity value of samples are displaced in fig .13. As prepared samples(x=0, 0.25, 0.5, 0.75) exhibit higher value of electrical conductivity than that of undoped Calcium cobalt oxide. The enhancement in electrical conductivity is due to the increase in charge carriers and sr^{+2} ion in the system. The samples displayed nearly identical behavior across the measured temperature range, as evidenced by the curve depicting electrical conductivity versus temperature which shows metallic like behaviour below 300 ^{O}C, semiconductor like behaviour between 300 ^{O}C to 520 ^{O}C , and metallic like behaviour after 520 ^{O}C. this may be due to an incommensurate spin density wave (IC-SDW) from semiconducting like to metallic like one. In any case the lowest measured electric conductivity is 97.899 S.cm^{-1} at 500 ^{O}C . the highest electrical conductivity obtained from Sr doped $Ca_3Co_4O_9$ is 153 S.cm^{-1} Which IS 18% higher then the undoped $Ca_3Co_4O_9$.since the conductivity is directly proportional to the carrier concentration, the conductivity can increase with increasing the concentration of Sr Which shown in the FIG:13.

The electrical conductivity first increased and then decreased with temperature for all samples depicting a metal to insulator transition. Furthermore, a change in the metal to insulator transition temperature was observed in the samples prepared. The metallic conduction can be explained with the movement of electrons from t_{2g} orbital to e_g orbital so as to fill eg orbital. This will widen the example orbital bandwidth and hence aid to a metallic transport in the prepared samples.

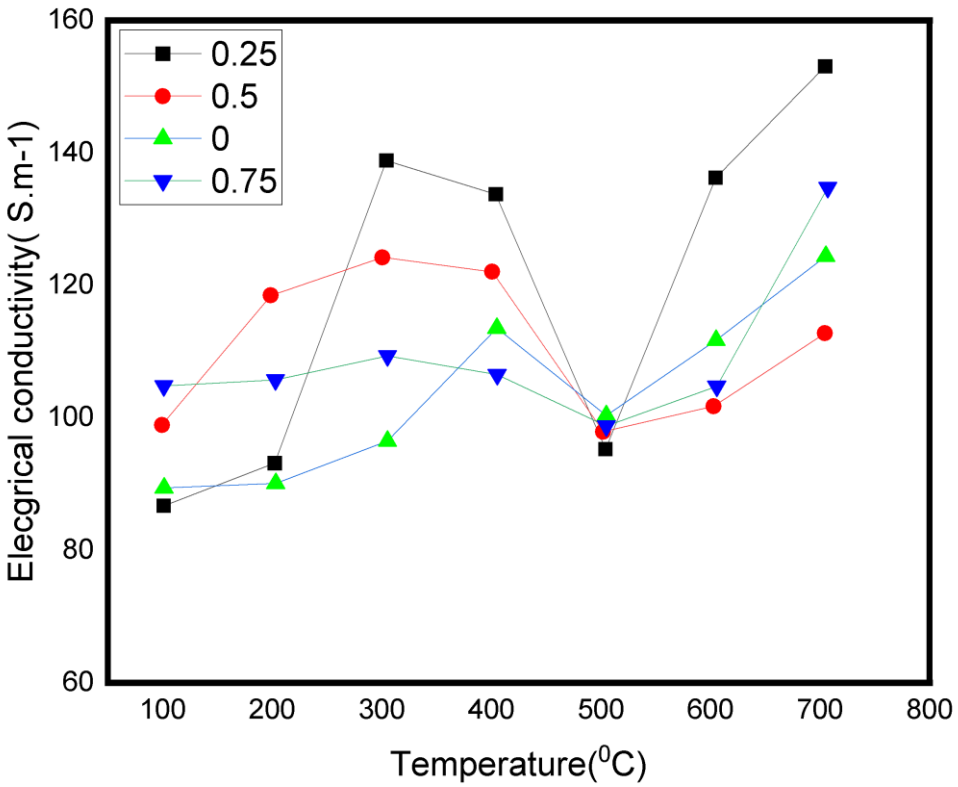

FIG:13. Temperature dependence of electrical conductivity of Ca3-xSr xCo4O9 sample

3.3 SEEBECK COFFICENT

The evolution of absolute values of Seebeck coefficient with temperature is given in figure Fig :14. The positive values of the Seebeck coefficient observed across the measured temperature range for all samples confirm a p-type conduction mechanism dominated primarily by holes. Additionally, the Seebeck coefficients of all samples exhibit a monotonic increase as temperature rises. It's notable that the Seebeck coefficient rises with the augmentation of Sr doping, except for when x=0.5, shown in Fig.14. The highest measured Seebeck coefficient of 270.07μVK-1 at 750 OC for CCO-Sr0.75 surpasses that of the undoped sample prepared in this study by 23%. The enhanced Seebeck coefficient in doped samples is attributed to two main factors. Firstly, Sr occupying the Ca site introduces point defects that scatter low-energy carriers, thereby improving the Seebeck coefficient. Secondly, since Sr is heavier than Ca, its doping may increase the effective mass, further contributing to a higher Seebeck coefficient. The expression for the dependence of S on carrier concentration(n) is given as follows:

$$S = -\frac{\pi 2 k 2}{3e} T \left(\frac{N(E)}{n}\right) + \text{const}$$

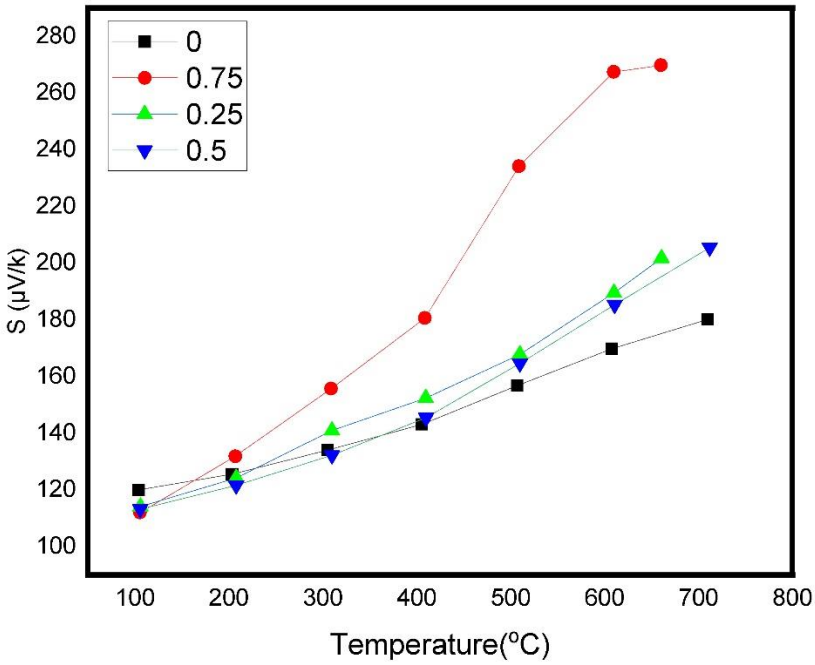

FIG:14 Seebeck Coefficient of $Ca_{3-x}Sr_xCo_4O_9$ sample with temperature

the sample with x=0.75 demonstrates the highest Seebeck coefficient, despite having a comparatively low carrier concentration. This phenomenon occurs due to the interplay between carrier concentration and mobility in thermoelectric materials.

When the carrier concentration decreases in a p-type semiconductor, the Seebeck coefficient tends to increase if the reduction in carrier concentration is not offset by a significant decrease in mobility. This is because a lower carrier concentration diminishes the electronic contribution to thermal conductivity, allowing the lattice contribution to become more dominant. Consequently, this shift in dominance often leads to an increase in the Seebeck coefficient.

3.4. POWER FACTOR

To assess the thermoelectric performance of these materials, the power factor (PF) has been computed, and its temperature dependence is illustrated in Figure 15. Power factor of each composition can be determined by multiplying electrical conductivity with square of Seebeck coefficient.

$$\text{Power factor} = S^2 \sigma$$

From the graph we can observe that the power factor are enhanced in the entire experimental doping range ($0 < x < 0.75$) the highest PF value of $1.4 mW^{-1}k^{-2}$ appears as X is 0.75 measuring at 700 ^{O}C, which is 40 % higher than that of undoped one. Therefore, X=0.75 The notion of a

transitional point concerning the Sr doping content is considered.

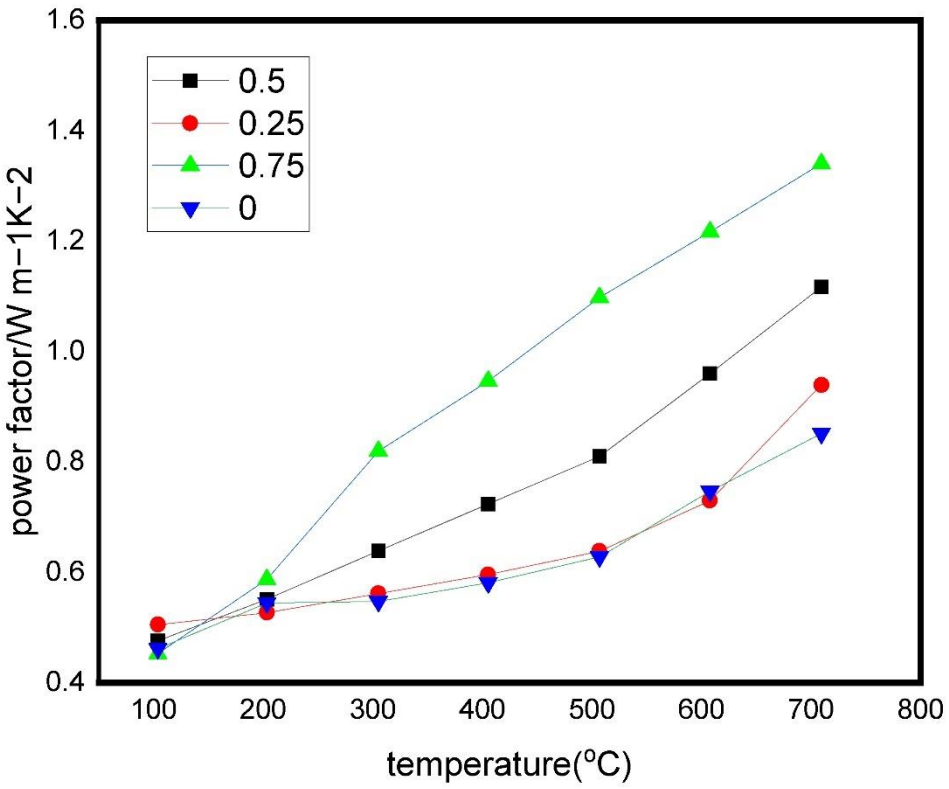

Figure:15. Variation in power factor of $Ca_{3-x}Sr_xCo_4O_9$ samples

CHAPTER 4

CONCLUSION

Strontium Substitued $Ca_3Co_4O_9$ sample were prepared using solid state reaction method. Diffraction peacks of all the samples prepared belongs to monoclinic structure with C1M1 space group. The electrical conductivity values were found to be increased with Sr substitution and a maximum of 153 $S.cm^{-1}$ was observed around 700 ^oC for $Ca_{2.25}Sr_{0.75}Co_4O_9$. Seebeck coefficients increases with Sr substitution due to its directly dependence on carrier concentration. A maximum power factor value that obtained after doping is 1.4$mW^{-1}k^{-2}$ for x= 0.75 sample at 700 ^oC.

Referances

1. Donald J.Wuebbles, SwarnaliSanyal; Air Quality in a Cleaner Energy world, Springer-Curr Population Rep (2015)1:117-129.

2. Terry M.Tritt and M.A. Subramanian: Thermoelectric Material Phenomena and Application; A Bird Eye View, MRS BULLETIN- Volume 31 (March-2006).

3. K.Rademann, V.S.Raghuwanshi, A.Hoell; Chapter-3 Crystalliation and Growth mechanisms of Nanostructures in silicate Glass: From Complete Characteriation Toward Applications; William Andrew ASP, Glass Nano composites Synthesis, Properties and Applications, 2019, pages 89-114

4. ShariarShafiee, Topal; When will fossil fuel reserves be diminished? –Elsevier, Energy Policy37-2009-181-189.

5. P.Pichanusakorn, P.Bandaru, Nanostructured thermoelectrics, Mater.Sci.Eng.R67 (2010)19-63.

6. Xiao Zhang, Li-Dong Zhao,Thermoelectric Materials- Energy conversion between heat and electricity-Sciences Direct –journal of materiomics 1(2015)92-105.

7. Prashantha.K,Sonam Wango, Smart power generation from waste heat by thermoelectric generator, International Journal of Mechanical and Production Engineering, Sep (2016).

Yong Du, JiayueXu, Biplab paul, Per Eklund- Flexible thermoelectric materials and devices Elsevier-Applied Materials Today-12(2018)366-388.

8. Xiaoyuanhou,Yanci Yan, Xu Lu; Routes for high- performance thermoelectric material-Elsevier-Materials Today- Volume 21, Number 9,Nov(2018)

9. Wenk, Hans-Rudolf, Bulakh, Anderi-Minerals- their constitution and orgin, Ny, Cambridge University press P.413 (2004).

13. Qingdi Zhou, Brendan J. Kennedy, Thermal expansion and structure of Orthorhombic CaMnO3-Science Direct-Journal of Physics and chemistry of solids 67(2006)1595-1598.

14.Shafiei, Rahul A.Salim, Non-renewable and renewable energy consumption and Co2 emission in OECD countries: A Comparative Analysis. Energy policy 66 (2014)547-556.

15. RosiF.D., Thermoelectric seebeck coefficient of two –dimensional electron gas in nature materials, 2007.6(2):129-134.

16. Wood Lockwood A, Chmielewski A,Parker J. Zoltan A.High temperature hall effect apparatus. RevSci Instrum 1984; 110-3

17. Goldsmith HJ.Introduction to thermoelectricity. Heidelberg: Springer; 2010.

18. Hibble S J.Cooper Sp,Hannon Ac, Fawcett I D and Greenblatt MJ 1999 J. PHYS. Condens.Matter 11 1921.

19. Ling C D, Neumeier J J and Argyriou DN 2001 J. Solid state chem.160-162.

20. Lufaso M W and Woodward P M 2001 Acta Cryst.B57.

21. A.R. West, Basic solid state chemistry, John Wiley &sons, 1999.

22. The Infracord double- beam spectrophotometer''. Clinical Science. 16(2).1957.

23. Y. Zhu, C. Wang, and J. Liu, 'Enhanced Thermoelectric Response at High Temperature', no. November, pp. 1–7, 2015.

24 T. Yang and T. Cheng, 'RSC Advances', RSC Adv., vol. 7, pp. 44659–44664, 2017.

25. Wu T, Tyson TA, Bai J, Pandya K, Jayed C, Fischer D (2013) On the origin of enhanced thermoelectricity in Fe doped $Ca_3Co_4O_9$. J Mater Chem C 1:4114–4121

26. Constantinescu G, Rasekh Sh, Torres MA, Bosque P, Diez JC, Madre MA, Sotelo A (2015) Effect of Na doping on the $Ca_3Co_4O_9$ thermoelectric performance. Ceram Int 41:10897–10903

27. Wang D, Chen L, Yao Q, Li J (2004) High-temperature thermoelectric properties of $Ca_3Co_4O_{9+\delta}$ with Eu substitution.

28.Moser D, Karvonen L, Populoh S, Trottmann M, Weidenkaff A (2011) Influence of the oxygen content on thermoelectric properties of $Ca_{3-x}Bi_xCo_4O_{9+\delta}$ system. Solid State Sci 13:2160–2164

29. Pei J, Chen G, Lu DQ, Liu PS, Zhou N (2008) Synthesis and high temperature thermoelectric properties of $Ca_{3-x-y}Nd_xNa_yCo_4O_{9+\delta}$. Solid State Commun 146:283–286

30. Liu HQ, Zhao XB, Zhu TJ, Song Y, Wang FP (2009) Thermoelectric properties of Gd, Y co-doped $Ca_3Co_4O_{9+\delta}$. Curr Appl Phys 9:409–413

31. Zhang Z, Zhang C, Liao Q, Qin L, Deng Y, Liang L (2022) Optimizing electrical and thermal transport properties of $Ca_3Co_4O_9$ based thermoelectric materials by Ag and Fe co-addition. Mater Today Commun 33:104866

32, Zhang FP, Lu QM, Zhang JX (2009) Synthesis and high temperature thermoelectric properties of $Ba_xAg_yCa_{3-x-y}Co_4O_9$ compounds. J Alloys Compd 484:550–554

33. Hao H, Zhao L, Hu X (2009) Microstructure and thermoelectric properties of Bi- and Cu-substituted $Ca_3Co_4O_9$ oxides. J Mater Sci Technol 25:105–108

34. Bhaskar A, Huang YC, Liu CJ (2014) Thermoelectric properties of $Ca_{3-x}Ag_xCo_{3.95}Fe_{0.05}O_9+\delta$ ($0 \leq x \leq 0.3$). J Electron Mater 43:535–540

35. Ou Y, Peng J, Li F, Yu ZX, Ma FY, Xie SH, Li J-F, Li JY (2012) The effects of dual doping on the thermoelectric properties of $Ca_{3-x}M_xCo_{4-y}Cu_yO_9$ (M = Na, La). J Alloys Compd 526:139–144.

36. Hira U, Han L, Norrman K, Christensen DV, Pryds N, Sher F (2018) High-temperature thermoelectric properties of Na- and W-doped $Ca_3Co_4O_9$ system. RSC Adv 8:12211–12221.

36.Tang GD, Yang WC, He Y, Wang ZH (2015) Enhanced thermo electric properties of Ca3Co4O9+δ by Ni, Ce co-doping. Ceram Int 41:7115–7118